# MICROANALYSIS OF OXIDE SURFACE LAYERS BY MEANS OF THE NUCLEAR REACTION $^{18}O(p, \alpha)\,^{15}N$

BY A. TUROS, L. WIELUŃSKI

Institute of Nuclear Research, Warsaw*

AND J. JELIŃSKA

Institute of Experimental Physics, University of Warsaw**

*(Received July 15, 1972; Revised paper received November 21, 1972)*

A method to determine the distribution of oxygen in surface layers is described. The experiment consists in measuring the yield of the $^{18}O(p, \alpha)^{15}N$ reaction as a function of the incident proton energy in the vicinity of the 629 keV resonance. Distribution profiles of oxygen are obtained by comparison of the experimental data with the yield curve calculated on a theoretical basis. This technique was applied to study the oxide surface layers made by anodic oxidation of aluminium. Due to the large reaction cross-section and lack of parasitic reactions the method is applicable even to the samples, which are not enriched in the isotope $^{18}O$. Determination accuracy of oxygen concentration is better than 5% and the depth resolution is 300 Å.

## *1. Introduction*

Oxidation processes are of great importance in various branches of modern science and technology. The most spectacular example is that of solid state electron technology. Oxide surface layers are widely used in silicon integrated device technology as dielectric isolation, impurity masking during diffusion, surface passivation and active device dielectric.

Studies of the phenomena occurring during the oxidation of surfaces are of great interest in other fields of solid state physics and technology including metallurgy, electrochemistry, electronic components industry *etc.*

Precise examination of the oxide films structure, being generally of practical interest *i.e.* of thicknesses below 1 μm is a rather difficult task.

* Address: Instytut Badań Jądrowych, Hoża 69, 00-681 Warszawa, Poland.

** Address: Instytut Fizyki Doświadczalnej, Uniwersytet Warszawski, Hoża 69, 00-681 Warszawa, Poland.

Using optical methods such as interference microscopy [1] or ellipsometry [2] one can measure the thickness of the surface layer. It is, however, more difficult to find the method for the purpose of quantitative analysis of oxygen in the surface layers. This is mainly due to the very small quantities of oxygen involved, which are usually in the sub-microgram range. For this reason mass spectrometry is precluded because it is practically impossible to convert such small quantities of oxygen to a gas. Infrared spectroscopy has low sensitivity in the case of oxygen and its use is limited to some special cases [3].

Recently electron microscopy has been succesfully applied to the investigation of oxide layers [4] although it is rather difficult to obtain some quantitive results.

Neutron activation analysis is hardly applicable for oxygen. This is due to the very short life times of activation products. The longest life time among the products of oxygen activation is that of $^{19}O$ (29 s.). The $^{19}O$ isotope can be produced by the $^{18}O(n, \gamma)\,^{19}O$ reaction [5].

More practical is the activation by charged particles [6–8]. The use of this technique requires, however, bombarding energy of the particles above 3 MeV. It means that a cyclotron or large Van de Graaff accelerator should be used. Special precautions against radioactive products of competing reactions, should be undertaken. This involves very often a fairly complex process of chemical separation.

Nuclear reactions and elastic scattering techniques provide an alternative method for microanalysis of surface layers. The method is based on the direct observation of the charged particles produced or scattered in the investigated sample. The bombarding particles used are low energy (0.5–2 MeV) hydrogen or helium ions usually accelerated in small Van de Graaff accelerators.

Nuclear reactions were first applied to the study of surface layers by Amsel and Samuel [9]. Recently this technique was applied to detection of light elements in surface layers ($^{10}B$, $^{12}C$, $^{14}N$, $^{16}O$, $^{18}O$, and $^{19}F$) [10–16].

In contrast to the nuclear reactions, elastic backscattering of heavy charged particles is mainly used in the analysis of surface layers containing medium and heavy elements [17, 18]. Recently Meyer *et al.* [19] have combined the backscattering technique with the directional effects which occur when the incident beam is aligned with one of the single crystal axes (channeling effect). This makes it possible to analyze the distribution of low $Z$ elements on the crystal surface.

One of the greatest advantages of the nuclear reactions and backscattering techniques is the possibility of the position determination of a given element inside some other material.

In the case of elastic backscattering or nonresonant nuclear reaction, the concentration profile can be deduced from the shape of the outgoing particles energy spectra [16, 20]. The better depth resolution is to be obtained using nuclear resonance reactions provided that the resonance is isolated and its width is less than several keV [14].

In this paper we discuss the application of the 629 keV resonance of the nuclear reaction $^{18}O(p, \alpha)^{15}N$ to the determination of the oxygen concentration profile in $Al_2O_3$ surface layers obtained by anodic oxidation of aluminium.

## 2. *Principles of the method*

The concentration profiles of elements in which nuclear resonance reactions occur can be determined by the measurements of the reaction yield as a function of the incident particles energy in the vicinity of the resonance energy.

The number of particles emitted from a layer $dx$ at the depth $x$ for the incident particle energy $E_0$ is given by

$$dN = I\Omega\sigma\left(E_0 - x\left|\frac{dE}{dx}\right|\right)C(x)dx \tag{1}$$

where: $I$ — number of incident particles, $\Omega$ — solid angle of the detector acceptance, $\sigma(E)$ — differential cross-section of the reaction, $C(x)$ — concentration profile, *i.e.*, the number of given kind nuclei per cm$^3$ at the depth $x$ of the sample, $\frac{dE}{dx}$ — stopping power of incident particles in the target material.

In the case where exists an isolated, large narrow resonance in the excitation curve, nearly all detected particles are produced at the depth interval $x$ in the vicinity of the depth $x_R$ at which the resonance energy $E_R$ is attained

$$x_R = (E_0 - E_R)\left|\frac{dE}{dx}\right|^{-1}. \tag{2}$$

The depth interval $\Delta x$ corresponds to the main part of a resonance with a width $\Gamma$ *i.e.*

$$\Delta x = 2\Gamma\left|\frac{dE}{dx}\right|^{-1}.$$

In practice this is a good first approximation. The counting rate $N(E_0)$ can be therefore computed by integration of Eq. (1)

$$N(E_0) = I\Omega\int_{E_R-\Gamma}^{E_R+\Gamma} C[x(E)]\sigma(E)\left|\frac{dE}{dx}\right|^{-1} dE. \tag{3}$$

By assumption that the concentration profile is a slowly changing function of $x$ (*i.e.* $C(x) \cong$ const.) in the depth interval $\Delta x$, and $\sigma(E)$ is given by the Breit-Wigner dispersion relation, one obtains

$$N(E_0) = 1.1\, I\Omega\sigma(E_R)C(x)\left|\frac{dE}{dx}\right|^{-1}\Gamma \tag{4}$$

$N(E_0)$ is therefore proportional to the average concentration $C(x)$ in the depth interval $\Delta x$.

The concentration profile can be obtained by measuring the reaction yield, step by step, at different energies of incident particles. Fig. 1 shows the principle of concentration profile measurements using the narrow isolated resonance.

The resonances of the nuclear reactions induced by charged particles are seldom really isolated. They are very often located on slowly changing background, which is

caused by the neighbouring resonances and/or different reaction mechanism. It is convenient in this case to divide the reaction cross-section into two parts *i.e.*

$$\sigma(E) = \sigma_S(E)+\sigma_R(E)$$

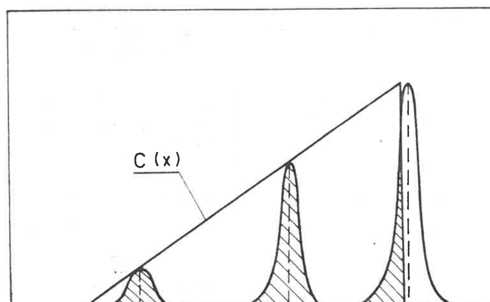


Fig. 1. Principle of the concentration profile measurements using narrow isolated resonance

where: $\sigma_R(E)$ and $\sigma_S(E)$ are the resonant and slowly changing parts of the cross-section, respectively.

The part of the observed yield due to $\sigma_S(E)$ is equal to

$$N_S(E_0) = I\Omega \int_0^{\infty} \sigma_S(E)C[x(E)] \left| \frac{dE}{dx} \right|^{-1} dE. \tag{5}$$

The quantity $N_S(E_0)$ is practically independent of the incident energy. The total observed yield $N_t(E_0)$ is therefore the sum of two parts

$$N_t(E_0) = N(E_0)+N_S(E_0), \tag{6}$$

$N(E_0)$ being given by Eq. (4).

As the information on the concentration profile is given in the $N(E_0)$, $C(x)$ can be deduced from Eqs (4) and (6).

$$C(x) = \frac{[N_t(E_0)-N_S(E_0)] \left| \frac{dE}{dx} \right|}{1.1\, I\Omega\sigma(E_R)\Gamma}. \tag{7}$$

The contributions to the observed yield due to both parts of the cross-section are schematically shown in Fig. 2.

In reality the method presented above should be considered as a first approximation only. To assure higher accuracy of measurements some other factors should be taken into account. These are:

the exact shape of the excitation curve $\sigma(E)$,

the shape of the incoming beam energy distribution $W(E_0, E_1)$,

the energy straggling of incident particles in the target material $S(E_1, E, x)$.

Thus, the relation between $N(E_0)$ and $C(x)$ can be obtained by the convolution of all functions involved.

$$N(E_0) = I\Omega \int_0^{\infty} \int_0^{\infty} \int_0^{x_0} W(E_0, E_1)S(E_1, E, x)\sigma(E)C(x)dxdEdE_1 \tag{8}$$

where $x_0$ is the thickness of the surface layer.

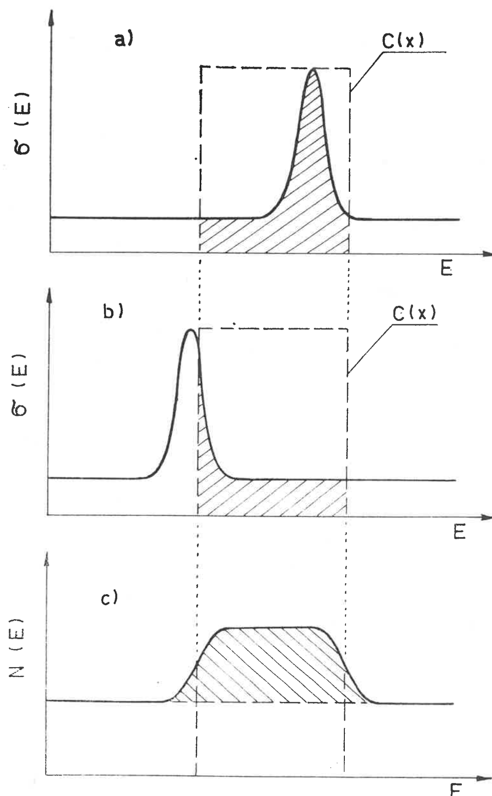


Fig. 2. Principle of the concentration profile measurements using narrow resonance located on constant background. Shaded areas in the excitation curve (a and b) are proportional to the reaction yield measured at various energies of incident particles. Shaded area in the yield curve (c) shows the contribution from the resonant part of the excitation curve

Let us now consider in detail the nature of each of the $\sigma$, $S$ and $W$ functions.

Because of the interference between the resonance and slowly changing parts in the excitation curve, the shape of the resonance differs from that described by the Breit--Wigner formula. The exact shape of the excitation curve can be obtained as a result of measurements using very thin target $\left(x_0 < \Gamma \left|\frac{dE}{dx}\right|^{-1}\right)$. The energy spread of the incident beam is described by the function $W(E_0, E_1)$. $W(E_0, E_1)$ is the probability that an incident

particle in the bombarding beam of average energy $E_0$ will have an energy between $E_1$ and $E_1+dE_1$. As was shown by Marcinkowski [21] the beam energy distribution out of the magnetic analyzer is nearly rectangular in shape.

The energy straggling is described by the function $S(E_1, E, x)$, which is the probability for an incident particle to have an energy between $E$ and $E+dE$ at a depth in the target between $x$ and $x+dx$. The theory of Tchalär [22], which describes the evolution of the

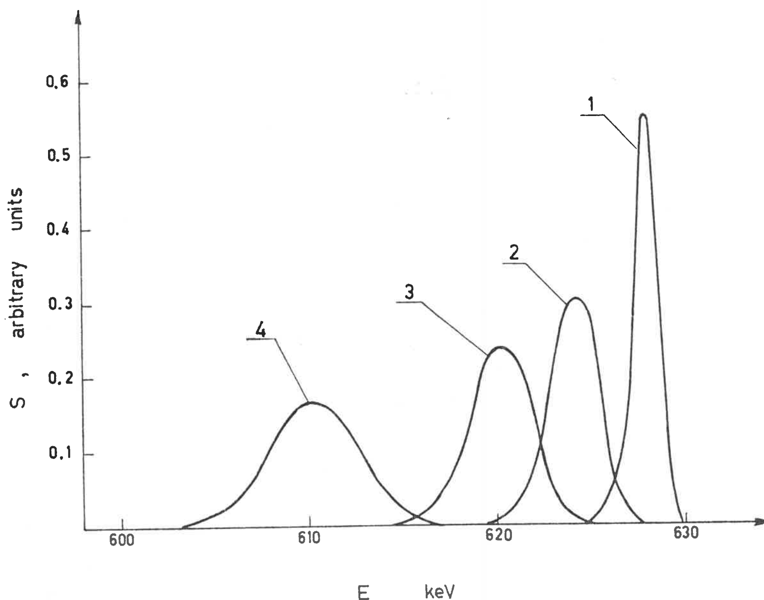


Fig. 3. Calculated energy distributions for protons of initial energy $E_0$ = 630 keV after passage various path lengths in $Al_2O_3$ : *1* — 200 Å, *2* — 600 Å, *3* — 1000 Å, *4* — 2000 Å

shape of the straggling distribution as a function of the mean energy loss of a particle, was used. The results of calculations based on Tchalär theory, performed for low energy protons and $Al_2O_3$ targets are shown in Fig. 3. The direct determination of $C(x)$ by solving the integral equation (Eq. (8)) is a very difficult task. This can be done using high speed and large memory digital computers. However the accuracy of several percent can be reached by the method of successive approximations, which was used in the present work. This, however, will be discussed in detail in Section 5. Owing to its simplicity the calculations based on this method can be done even by means of small computers.

One of the most important parameters of the concentration profile determination method is the depth resolution $\Delta X$, which is defined by

$$\Delta X = (\Gamma^2+\sigma_{str}^2+\sigma_i^2)^{1/2} \cdot \left| \frac{dE}{dx} \right|^{-1}$$

where: $\sigma_{str}$ — dispersion of the straggling distribution, $\sigma_i$ — dispersion of the incident beam energy.

The quantity $\Delta X$ is considered as the depth interval in which the value of concentration can be determined independently. Because of the $\sigma_{str}$ dependence on the thickness $x$ traversed by the incident particles in the target, the depth resolution is a function of $x$. Fig. 4 shows the variation of the depth resolution calculated for the 629 keV resonance ($\Gamma = 2.5$ keV) of the nuclear reaction $^{18}O(p, \alpha)^{15}N$.

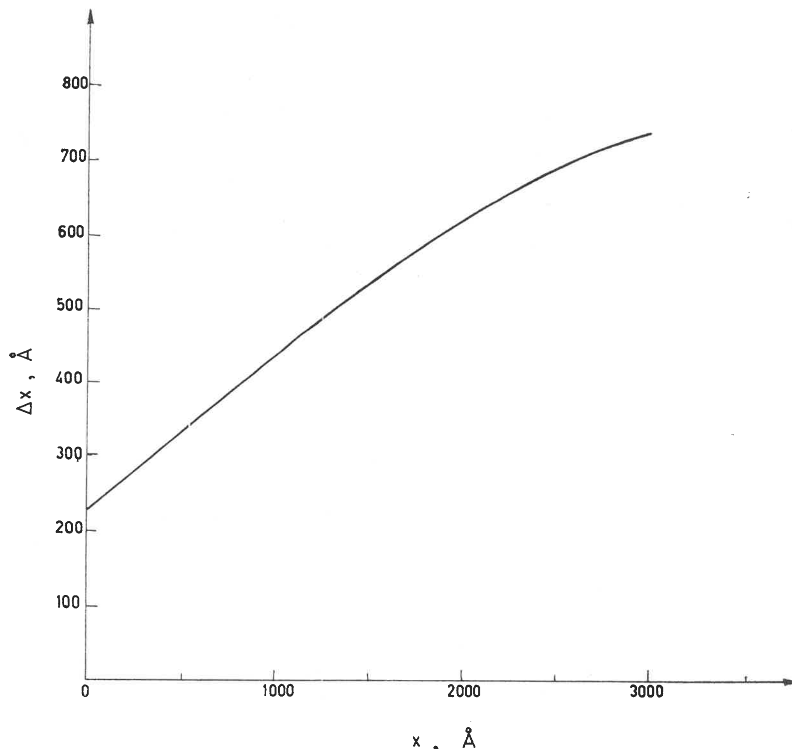


Fig. 4. Variation of the depth resolution with the $Al_2O_3$ surface layer thickness

### 3. *The nuclear reaction* $^{18}O(p, \alpha)^{15}N$

The $^{18}O(p, \alpha)^{15}N$ is an exceptionally convenient reaction for the nuclear microanalysis of oxide surface layers. The $Q$-value of this reaction is 3.970 MeV. At the incident proton energy of 630 keV the energy of $\alpha$-particles emitted at an angle of 150° is equal to 3.3 MeV and no $\alpha$-particles corresponding to excited states of $^{15}N$ are emitted.

Owing to the negative $Q$-value of the $^{16}O(p, \alpha)^{13}N$ reaction and small $Q$-value of the $^{17}O(p, \alpha)^{14}N$ reaction (1.19 MeV) there is no interference with these oxygen isotopes. This makes it possible to detect the $^{18}O$ nuclei in the natural oxygen in spite of its very low abundance (0.204%). The angular distribution of the $^{18}O(p, \alpha)^{15}N$ reaction is peaked in the backward direction, hence the angle of detection should be fixed possibly close to 180°. The excitation curve of this reaction, obtained with the 200 Å thick $Al_2O_3$ enriched up to 10% $^{18}O$ at an angle of detection $\theta = 150°$, is shown in Fig. 5.

The broad resonance at 830 keV ($\Gamma = 30$ keV) was used by Price and Bird [23] for lateral distribution measurements using highly collimated proton beam. It is, however, impracticable to use this particular resonance for concentration profile measurements.

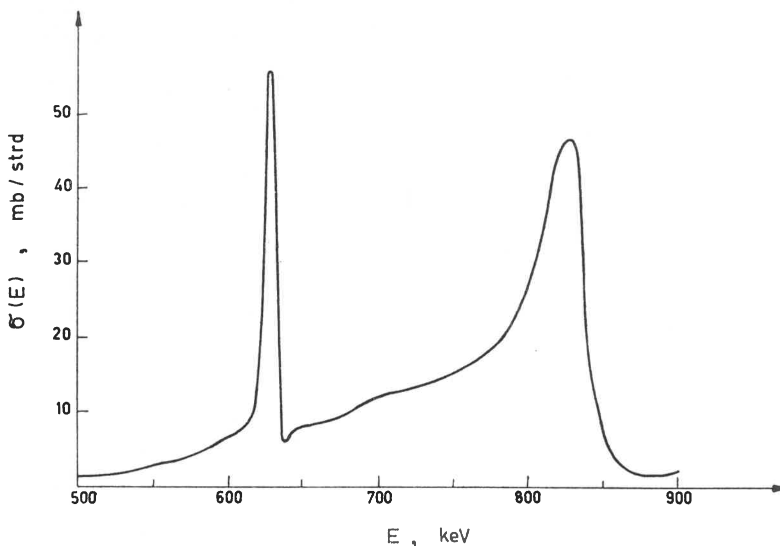


Fig. 5. Excitation curve of the $^{18}O(p, \alpha)^{15}N$ reaction measured at $\theta = 150°$

More advantageous is to use for purpose a much narrower ($\Gamma = 2.5$ keV) resonance at 629 keV.

Some other resonances in the 1000–2000 keV energy range may be also useful [14] although the cross-section in this energy range are about ten times smaller. This induced the necessity of the use of targets enriched up to 80–90% in the $^{18}O$ isotope.

## 4. *Experimental*

The proton beam was obtained from the Institute of Nuclear Research Van de Graaff accelerator. The beam has a diameter of 2 mm on the target and an estimated angular spread of less than $\pm 0.5°$. The energy of incident protons was changed by steps of 1–2 keV in the energy range sufficiently wide to cover the thickness of the measured target. In the case of 2000 Å thick $Al_2O_3$ target the incident energy was varied from 625 up to 690 keV.

The estimated energy spread of the incident beam was about 1 keV.

The $\alpha$-particles produced in the $^{18}O(p, \alpha)^{15}N$ reaction were detected at an angle $\theta = 150°$ by an silicon surface barrier detector subtending a solid angle of about 0.03 strd at the target. Protons scattered from the target were absorbed by 8 μm thick aluminium foil placed in front of the detector. The pulses due to $\alpha$-particles were analyzed by means of conventional electronic system including charge-sensitive preamplifier and linear amplifier coupled to the Intertechnique CA25/BM69 multichannel pulse height analyzer.

The construction of the scattering chamber used in our experiments is described in

detail elsewhere [24]. The $Al_2O_3$ targets were prepared by anodic oxidation of aluminium in $^{18}O$ enriched water containing ammonium citrate. The highest enrichment does not exceed 10%.

Some targets were made using an electrolyte which was not enriched in $^{18}O$. The thickness of the oxide layer formed by anodic oxidation is proportional to the applied voltage [25]. High purity, 20 μm thick aluminium foil was used.

Thickness of such targets is several times greater than the range of incident protons. Incident beam charge collected in the target was measured by the current integrator. In

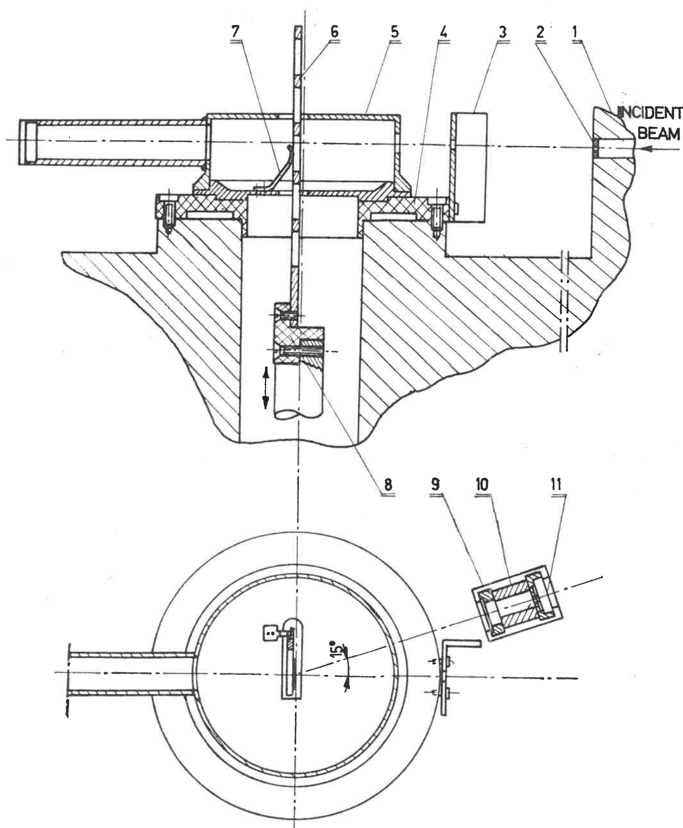


Fig. 6. Faraday cup. *1* — scattering chamber, *2, 3* — collimators, *4* — insulator disc, *5* — Faraday cup, *6* — target holder, *7* — contact spring, *8* — insulator (teflon), *9* — detector housing, *10* — magnet, *11* — detector

order to secure accurate measurements some precautions againts escape of secondary electrons should be made. For this purpose the Faraday cup of special construction was designed. This is shown on Fig. 6. The Faraday cup and 5-position target holder were electrically isolated from the rest of the scattering chamber. A long tubule was mounted at the back of the Faraday cup in order to avoid beam scattering effects when thin targets were used. The estimated accuracy of the beam charge measurements is about 2%. This is mainly determined by the accuracy of the current integrator.

### 5. *Results*

Figs 7 and 8 shown results of the yield measurements as a function of the incident proton energy obtained with $Al_2O_3$ targets enriched up to 8% in $^{18}O$.

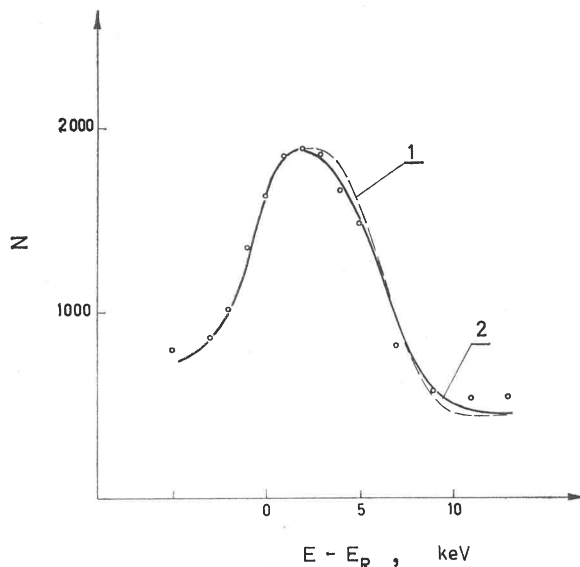


Fig. 7. Comparison between an experimental yield curve obtained for the 920 Å thick, uniform $Al_2O_3$ surface layer, enriched up to 8% in $^{18}O$ and calculated yield curve (*1* — without straggling, *2* — with straggling)

By the full line are shown the calculated yield curves corresponding to a uniform oxygen concentration *i. e.*

$$C(x) = \begin{cases} \text{const.} & x \leqslant x_0 \\ 0 & x > x_0, \end{cases}$$

where $x_0$ is the thickness of the oxide layer. Somewhat idealized yield curves, without straggling, are shown by dotted lines. It is clearly visible that the experimental points agree well with the solid curves. This similarity does not necessarily indicate that the oxygen concentration is really uniform, but simply that its variation is too slow to have any influence on the shape of the measured yield curve.

Rather large cross-section of the 629 keV resonance makes it possible to measure the concentration profile even by targets which are not enriched in $^{18}O$.

In Fig. 9 is shown the yield curve obtained by the $Al_2O_3$ target oxidized anodically in the electrolyte containing natural mixture of oxygen isotopes.

In order to test the sensitivity of the method, some targets with variable $^{18}O$ concentration were made. This was made in the following way: an aluminium foil was anodically oxidized at 20V in the electrolyte containing 2% of $^{18}O$ afterwards the electrolyte was removed and new electrolyte enriched up to 4% of $^{18}O$ is poured in, the sample is then oxidized at 40V. The same procedure was repeated for 6%/60V and finally for

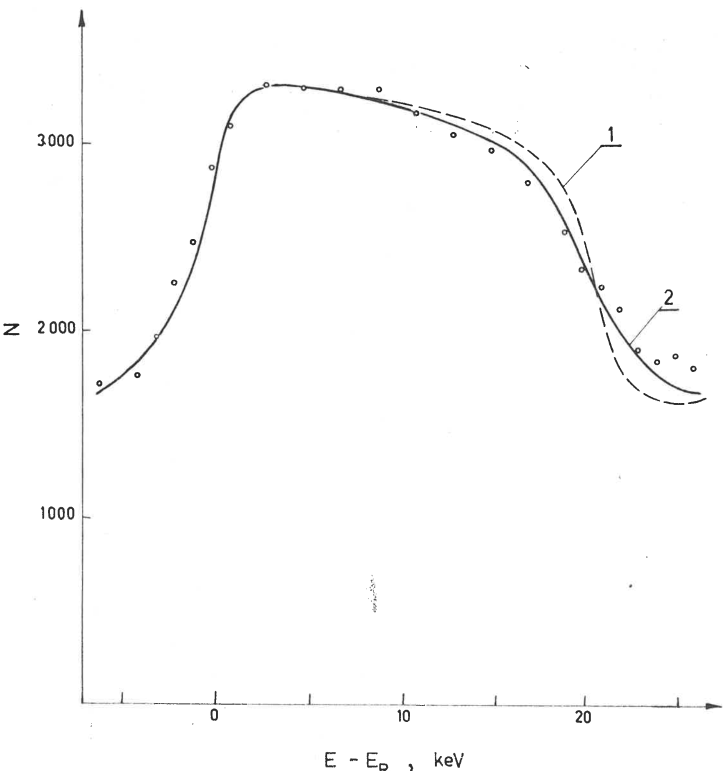


Fig. 8

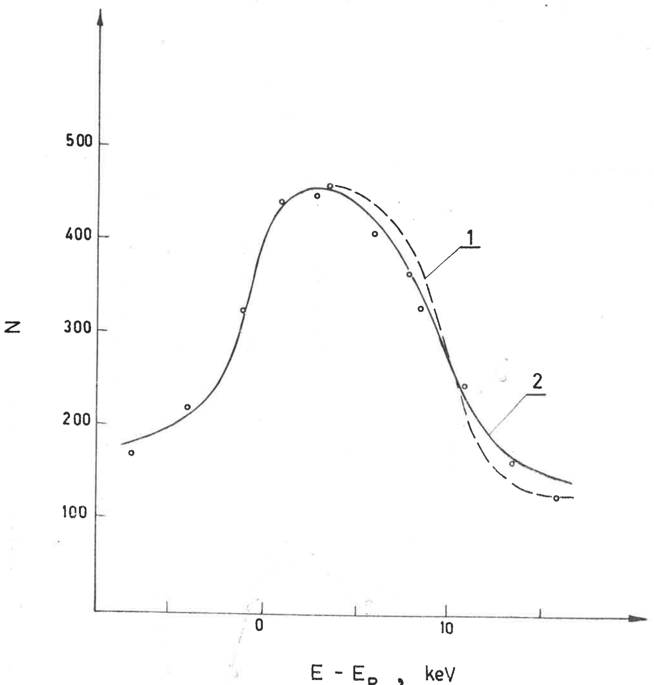


Fig. 9

Fig. 8. Comparison between the experimental yield curve obtained for the 2580 Å thick, uniform $Al_2O_3$ surface layer, enriched up to 8% in $^{18}O$ and calculated yield curves (*1* — without straggling, *2* — with straggling)

Fig. 9. Comparison between the experimental yield curve obtained for 1320 Å thick, uniform $Al_2O_3$ surface layer not enriched in $^{18}O$ (0.2% $^{18}O$) and calculated yield curve (*2*). The yield curve calculated without straggling is shown by dotted line (*1*)

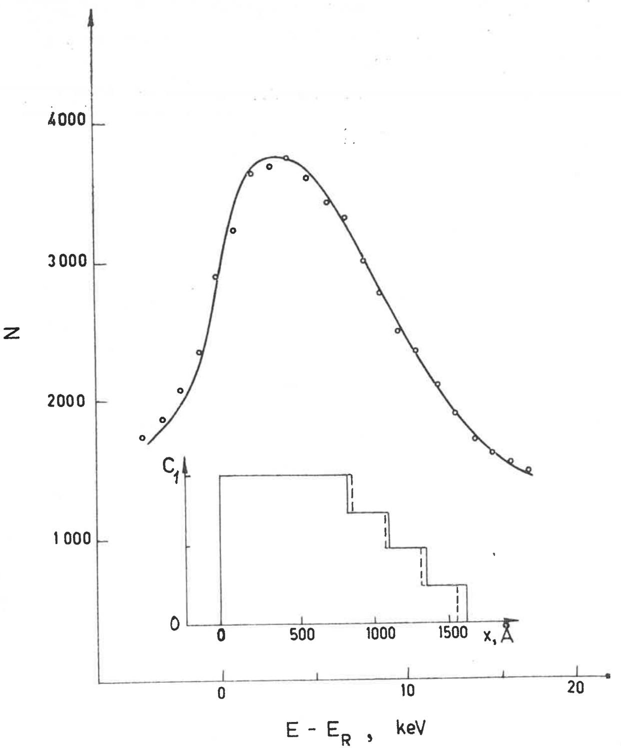


Fig. 10

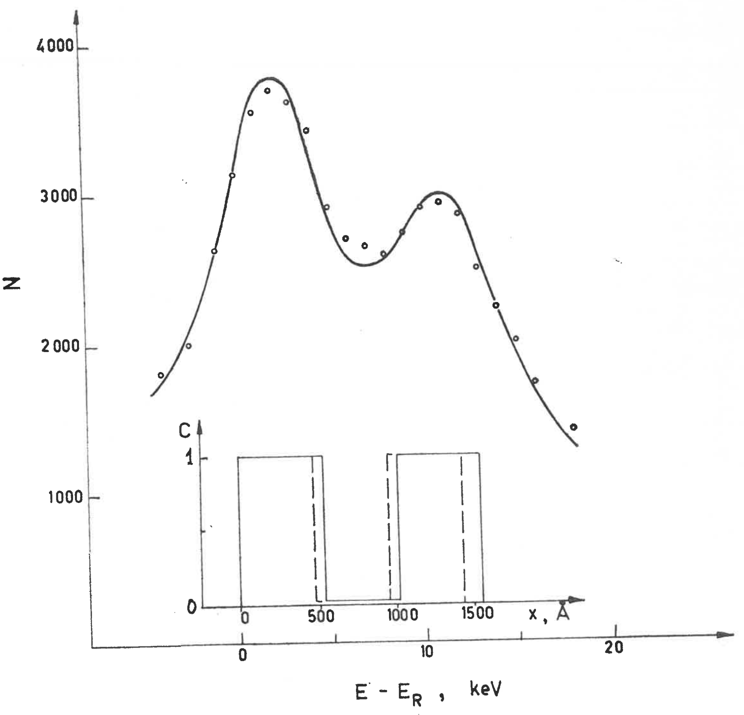


Fig. 11

Fig. 10. The yield curve measured for the $Al_2O_3$ surface layer of variable concentration of $^{18}O$. The line is the best fit to the experimental data. The insert shows the comparison between the calculated concentration profile (solid line) and that from anodic oxidation data (dotted line)

Fig. 11. The yield curve measured for the $Al_2O_3$ surface layer of variable concentration of $^{18}O$. The line is the best fit to the experimental data. The insert shows the comparison between the calculated concentration profile (solid line) and that from anodic oxidation data (dotted line)

8%/130 V. According to Amsel and Samuel [9] the $^{18}O$ concentration in a particular layer, which was formed by each step of anodic oxidation is not changed by the subsequent steps. In this way the step-like concentration profile of $^{18}O$ is obtained. In Fig. 10 are shown results of the measurements using such target.

Another concentration profile of $^{18}O$ was formed in the following oxidation scheme: 8%/40V + 0.2%/80V +8%/120 V. The yield curve measured by this target is shown

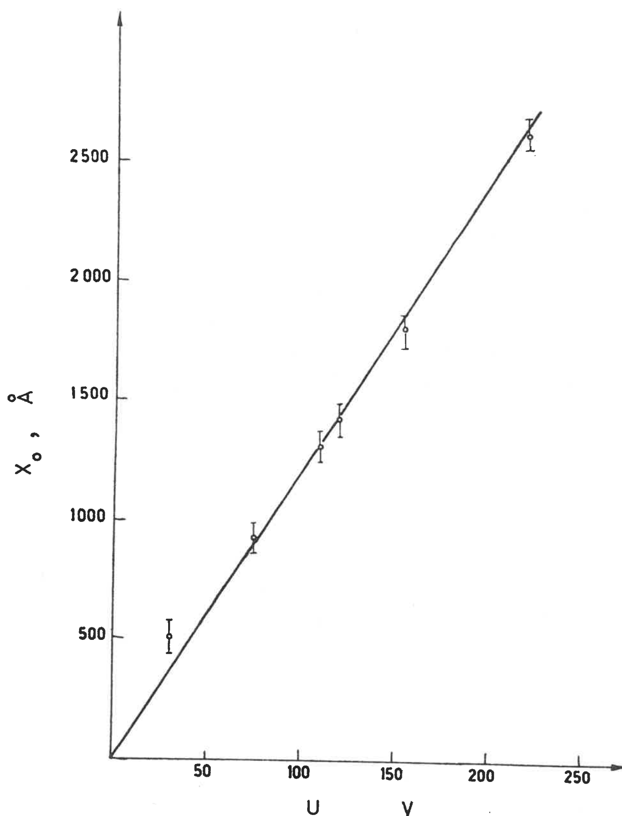


Fig. 12. Variation of the $Al_2O_3$ surface layers thickness as a function of the anodic oxidation voltage

in Fig. 11. The solid curves in parts of Figs 10 and 11 representing the concentration profile are the best fits of theoretical calculations based on Eq. (8) to the experimental points. This was made by the method of successive approximations. The starting form of the concentration profile $C(x)$ (first approximation) was obtained using Eq. (7). Next $C(x)$ was varied until the minimum of the $\chi^2$ value was obtained. $\chi^2$ was defined as usually

$$\chi^2 = \sum_{i=1}^{i=n} \frac{(N_i^{\mathrm{exp}} - N_i^{\mathrm{calc.}})^2}{N_i^{\mathrm{exp}}}$$

where: $n$ is the number of experimental points, $N_i^{exp}$ and $N_i^{calc}$ are experimental and alculcated yields respectively, corresponding to the energy $E_i$. The good agreement between the calculated profiles and that predicted from the anodic oxidation data (shown by dotted line in Figs 10 and 11) confirms the assumption of independent formation of each layer in the course of anodic oxidation.

Fig. 12 shows the variation of the thickness of uniform oxide layers with the voltage applied in anodic oxidation. The thicknesses are determined from the measured yield curves using the fitting procedure described above. The characteristic linear dependence of thickness *versus* voltage is clearly visible. The straight line in Fig. 12 has a slope of 12 Å/V. Results of the thickness measurements are strongly influenced by the accuracy of the proton stopping power data. The stopping power of aluminium and oxygen for protons in the 600–700 keV energy range calculated by Williamson *et al.* [26] are in good agreement with experimental data compiled by Bichsel [27] and were taken as a basis to the $Al_2O_3$ stopping power calculations. This can be done using the Bragg rule [28].

## 6. Conclusions

The experimental method described could be used in various fields of surface scientific and technological problems in which the processes of oxidation are involved. Owing to its great sensitivity and lack of parasitic reactions this method is applicable to the study of oxide layers, which are not enriched in the $^{18}O$ isotope. The accuracy of the concentration profile measurements is of the order of 5% with the depth resolution of 300 Å. The typical measurements time is about 6 hours. However, this number can be easily lowered by the use of a second detector and/or by enlarging the solid angle of detection.

The authors would like to thank Dr J. Turkiewicz for his continued interest in this work and R. Sochacka, M. Sc., for help in handling the samples.

## REFERENCES

[1] *Fundamentals of Silicon Integrated Device Technology*, R. M. Burger and R. P. Donovan Eds., Prentice-Hall Inc., New Jersey 1967.
[2] *Ellipsometry in the Measurement of Surface and Thin Films*, National Bureau of Standards, Washington 1964.
[3] J. R. Ligenza, W. S. Spitzer, *Phys. Chem. Solids*, **14**, 131 (1960).
[4] S. Yamazaki, I. Kagawa, *Japan J. Appl. Phys.*, **10**, 1028 (1971).
[5] T. Kamemoto, *Nature*, **203**, 513 (1964).
[6] R. Sippel, R. Glover, *Nuclear Instrum. Methods*, **9**, 37 (1960).
[7] S. S. Markowitz, J. D. Mahony, *Ann. Chem.*, **34**, 329 (1962).
[8] T. Nozaki, S. Tanaka, M. Furukawa, K. Saito, *Nature*, **190**, 39 (1961).
[9] G. Amsel, D. Samuel, *J. Phys. Chem. Solids*, **23**, 1707 (1962).
[10] A. Turos, L. Wieluński, J. Oleński, *Phys. Status Solidi*, (a) **16**, 211 (1973).
[11] E. Möller, L. Nilsson, N. Starfelt, *Nuclear Instrum. Methods*, **50**, 270 (1967).
[12] G. Amsel, D. Samuel, *Ann. Chem.*, **39**, 1689 (1967).
[13] G. Weber, L. Quaglia, *Nuclear Instrum. Methods*, **94**, 165 (1971).
[14] G. Amsel, J. P. Nadai, E. d'Artemare, D. David, E. Girard, J. Moulin, *Nuclear Instrum. Methods*, **92**, 481 (1971).

[15] E. Möller, N. Starfelt, *Nuclear Instrum. Methods*, **50**, 225 (1967).
[16] D. W. Palmer, *Nuclear Instrum. Methods*, **38**, 187 (1965).
[17] A. Turos, Z. Wilhelmi, *Nukleonika*, **13**, 975 (1968); *Nukleonika*, **14**, 319 (1969).
[18] A. Turos, L. Wieluński, *Nuclear Instrum. Methods*, **104**, 114 (1972).
[19] O. Meyer, J. Gyulai, J. W. Mayer, *Surface Sci.*, **22**, 263 (1970).
[20] G. Amsel, G. Beranger, B. de Gelas, P. Lacombe, *J. Appl. Phys.*, **39**, 2246 (1968).
[21] A. Marcinkowski, *Ph. D. Thesis*, Warsaw 1966 (unpublished).
[22] C. Tchalär, *Nuclear Instrum. Methods*, **61**, 141 (1968).
[23] P. B. Price, J. R. Bird, *Nuclear Instrum. Methods*, **69**, 277 (1969).
[24] A. Saganek, I. Śledzińska, A. Turos, Z. Wilhelmi, B. Zwięgliński, *Acta Phys. Polon.*, **B2**, 473 (1971).
[25] L. Young, *Anodic Oxide Films*, Academic Press, London and New York 1961.
[26] C. Williamson, J. P. Boujot, J. Picard, *Report CEA* — R 3042 (1968).
[27] H. Bichsel, *American Institute of Physics Handbook*, **8c**, McGraw-Hill, New York 1963.
[28] U. Fano, *Ann. Rev. Nuclear Sci.*, **13**, 1 (1963).